PROCEEDINGS OF SCIENCE

CBM at FAIR

Peter Senger*
GSI Darmstadt, Germany
E-mail: p.senger@gsi.de

Tatjana Galatyuk
GSI Darmstadt, Germany
E-mail: t.galatyuk@gsi.de

Anna Kiseleva
GSI Darmstadt, Germany, and PNPI RAS Gatchina, Russia
E-mail: a.kiseleva@gsi.de

Dmytro Kresan
GSI Darmstadt, Germany
E-mail: d.kresan@gsi.de

Evgeny Kryshen
SPbSPU, St. Petersburg, Russia
E-mail: e.kryshen@gsi.de

The Compressed Baryonic Matter (CBM) experiment will be one of the major scientific activities at the future Facility for Antiproton and Ion Research (FAIR) in Darmstadt. The goal of the CBM research program is to explore the QCD phase diagram in the region of high baryon densities using high-energy nucleus-nucleus collisions. The relevant observables and the layout of the proposed detector setup will be discussed.

The 3rd edition of the International Workshop — The Critical Point and Onset of Deconfinement —
July 3-7 2006
Galileo Galilei Institute, Florence, Italy

*Speaker.

© Copyright owned by the author(s) under the terms of the Creative Commons Attribution-NonCommercial-ShareAlike Licence.

PoS(CPOD2006)018

1. The future Facility of Antiproton and Ion Research (FAIR)

The future international Facility for Antiproton and Ion Research (FAIR) in Darmstadt will provide unique research opportunities in the fields of nuclear, hadron, atomic and plasma physics [1]. The accelerators will deliver primary beams (protons up to 90 GeV, Uranium up to 35 AGeV, nuclei with Z/A = 0.5 up to 45 AGeV) and secondary beams (rare isotopes and antiprotons) with high intensity and quality. The facility comprises a double-ring synchrotron, rings for accumulation, cooling and storage of primary and secondary beams, and dedicated detector arrangements. The research program includes the study of nuclei far from stability, hadron physics with antiproton beams, the study of compressed nuclear matter, the investigation of plasmas induced by ion and laser beams and atomic physics. First beams from SIS100/300 are scheduled for the years 2014/15. A sketch of FAIR together with the existing GSI facilities is presented in figure 1.

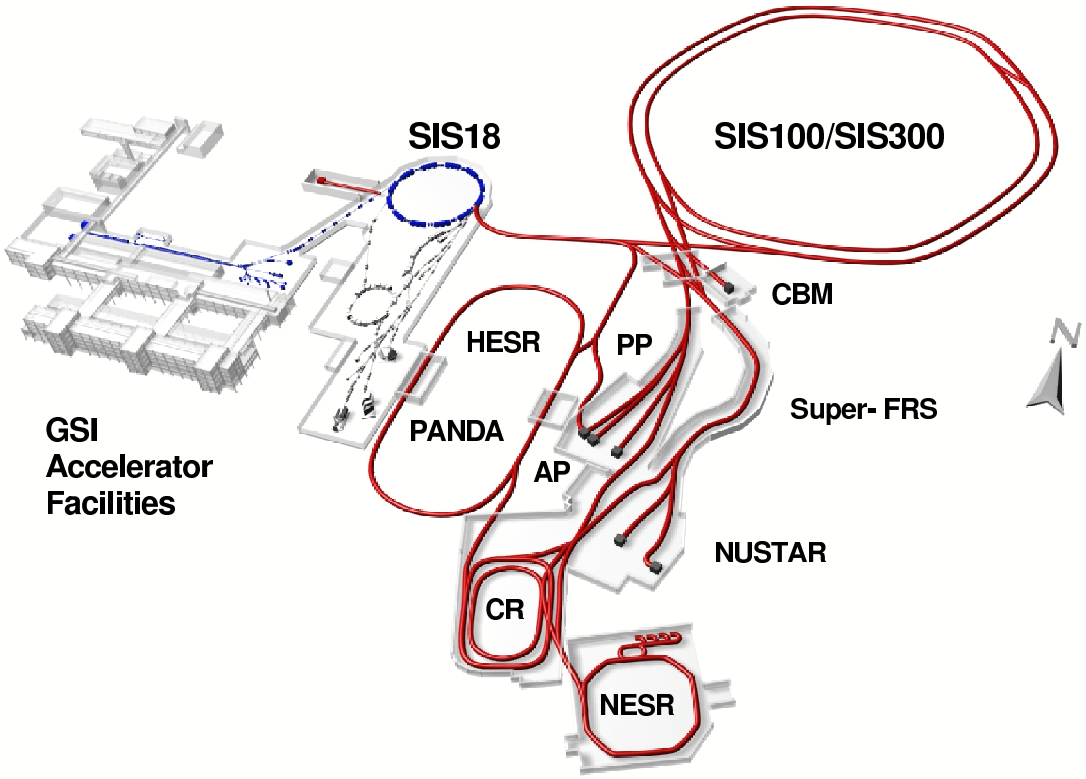

Figure 1: Layout of FAIR consisting of synchrotrons with rigidities of 100 Tm and 300 Tm (SIS100/300), the Superconducting Fragment Separator (SFRS), the storage rings for antiprotons (High-energy Storage Ring HESR), the Collector Ring (CR), and the New Experimental Storage Ring (NESR). The experimental facilities include the Compressed Baryonic Matter (CBM) detector to study high-energy nucleus-nucleus collisions, the PANDA detector for hadon physics experiments using cooled high-energy antiproton beams, the NUSTAR detectors used for experiments on the structure of unstable nuclei and on nuclear astrophysics, experimental setups for Plasma Physics (PP) and Atomic Physics (AP) [1]).

PoS(CPOD2006)018

2. Exploration of the QCD phase diagram

The FAIR beams will be available for many month per year for the Compressed Baryonic Matter experiment which aims at the exploration of QCD phase diagram at high net baryon densities and moderate temperatures. In this sense, the CBM approach is complementary to the studies of matter at high temperatures and low net baryon densities presently performed at RHIC and planned for LHC. At very high baryon densities, new phases of strongly interacting matter are expected to occur [2, 3, 4]. This exciting field of high baryon density QCD needs input from experimental data, which can only be provided by new and dedicated measurements. The CBM experiment is being designed for a comprehensive investigation of all relevant observables including strangeness, charm, and dilepton pairs.

Very high baryon densities - which are comparable to those in the core of neutron stars - are predicted to be reached in heavy-ion collisions already at moderate beam energies. This is illustrated in figure 2 (left panel) which depicts the density in the inner volume of central Au+Au collisions as function of time calculated with a transport code (quark gluon string model QGSM, see [5]). Already at a beam energy of 5 AGeV the baryon density exceeds a value of 1 fm^{-3}, i.e. more than 6 times saturation density. The corresponding energy density is plotted in the right panel of figure 2 as function of baryon density (in units of saturation density). At a beam energy of 5 AGeV the energy density is predicted to reach a value of 2 GeV fm^{-3} which is - according to lattice QCD calculations - already beyond the hadronic phase.

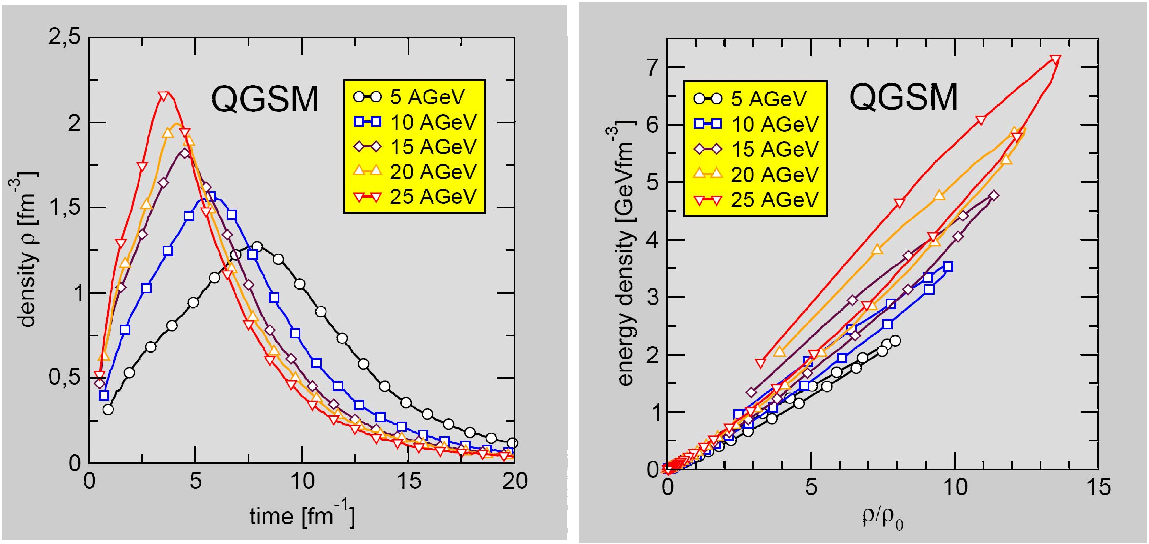

Figure 2: Left panel: nuclear density in the inner volume of central Au+Au collisions as function of time calculated with the Quark Gluon String Model QGSM for beam energies between 5 and 25 AGeV [5]. Right panel: Corresponding energy density as function of the baryon density (in units of saturation density.)

Trajectories of nucleus-nucleus collisions in the T - μ_B plane have been calculated with a 3-fluid hydrodynamics model [6]. Figure 3 depicts the trajectories corresponding to different beam energies. The phase diagram also contains the critical endpoint (star) which has been predicted recently by lattice QCD calculations [7, 8]. The lattice calculations find a first order phase transition above $\mu_B \approx 400$ MeV, and a smooth cross over from hadronic to partonic matter below this value.

PoS(CPOD2006)018

The hydrodynamics model calculation indicates that this critical endpoint might be found in the vicinity of the freeze-out point of a central Pb+Pb collision at a beam energy of about 30 AGeV.

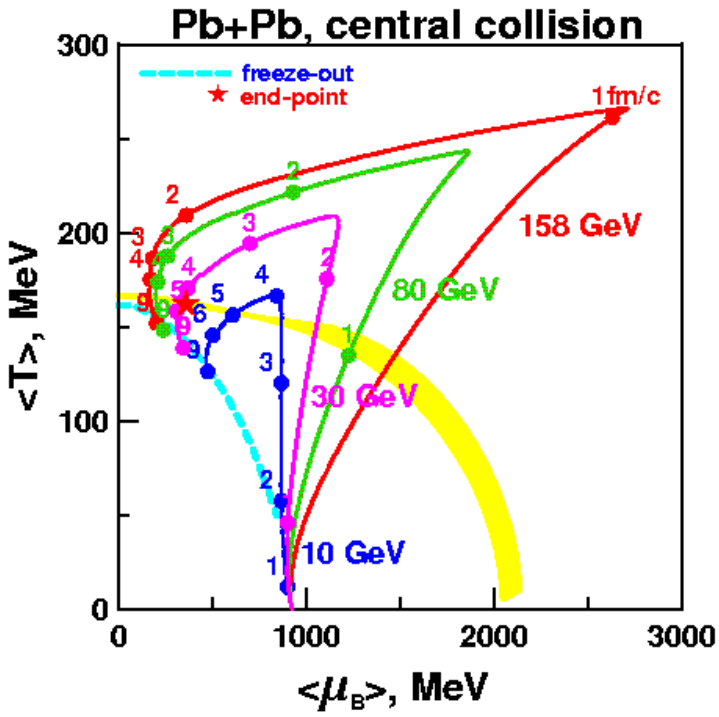

Figure 3: Trajectories of heavy ion collisions in the QCD phase diagram calculated by a 3-fluid hydrodynamics model [6]. Dashed line: chemical freeze-out curve. Star: critical end-point.

3. Experimental observables

The CERN-NA49 collaboration found a pronounced peak in the excitation function of the K^+/π^+ ratio in central Pb+Pb collisions at a beam energy of 30 AGeV [9]. This structure cannot be explained by any theoretical model. The Lambda/pion ratio exhibits also a maximum at the same beam energy. In this case, the shape of the excitation function can be reproduced by a statistical model analysis, which indicates that the transition from baryon dominated matter to meson dominated matter occurs at a beam energy of about 30 AGeV. It turns out that the maximum net-baryon density at freeze-out is reached at a beam energy of 30 AGeV [10]. Therefore, the FAIR energy range is well suited to search for the onset of chiral symmetry restoration, for the first order deconfinement phase transition and its critical endpoint, and to explore the equation of state of hadronic and partonic matter. The major challenge is to find and to measure observables which serve as sensitive diagnostic probes.

The onset of a first order phase transition is expected to cause a discontinuity in the excitation function of particular observables. A beam energy scan looking at a variety of diagnostic probes is needed to clarify the experimental situation. This includes the measurement of the phase-space distributions of strange particles, in particular multi-strange baryons (anti-baryons), and particles containing charm quarks. For example, a discontinuity in the excitation function of the J/ψ-to-ψ' ratio would indicate sequential charmonium dissociation due to color screening in the deconfined phase. Moreover, event-by-event fluctuations are expected to appear when crossing a first order phase transition, and particularly in the vicinity of the critical endpoint. The identification of a

PoS(CPOD2006)018

critical point would provide direct evidence for the existence and the character of a deconfinement phase transition in strongly interacting matter.

Figure 4 illustrates that in the FAIR energy range ($\sqrt{s_{NN}}$ = 2.7 - 9.4 GeV) only the yields of the most abundant particles (pions, kaons and lambdas) have been measured with sufficient statistics. Much less is known about the yields and phase-space distributions of multi-strange hyperons (and antihyperons), in particular information on their collective flow is lacking.

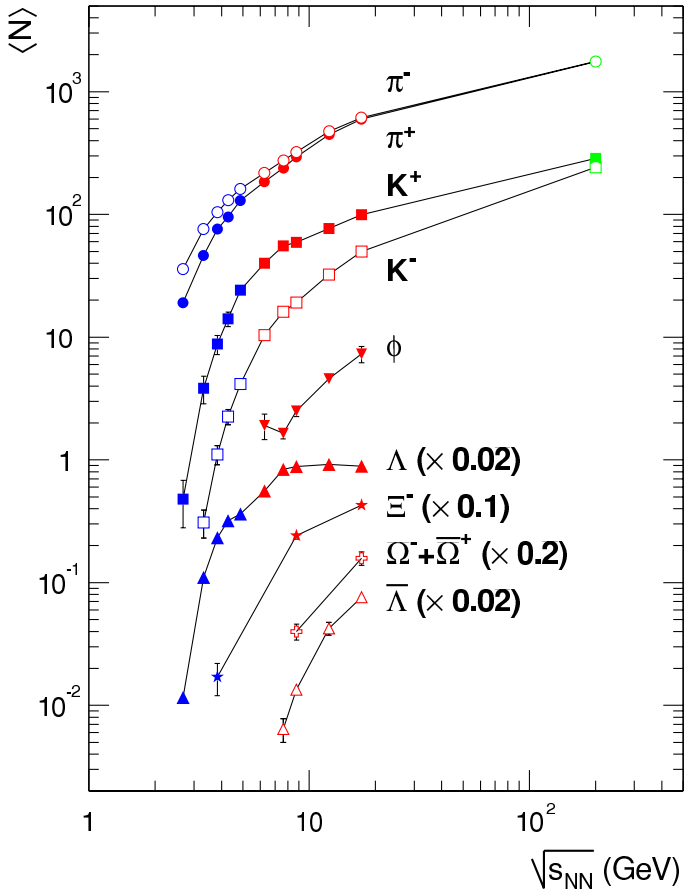

Figure 4: Multiplicities of mesons and hyperons measured in central Au+Au or Pb+Pb collisions as a function of the invariant energy $\sqrt{s_{NN}}$ (taken from Ref. [11])

3.1 Collective flow

As an example for the possible sensitivity of flow observables on the effective degrees of freedom in the early phase of the collision, the midrapidity elliptic flow v_2 for charged hadrons is displayed in Figure 5 as predicted by the AMPT transport model [12]. This hybrid model has the possibility to include a partonic phase ("string melting") before hadronization. Figure 5 presents the elliptic flow v_2 as function of transverse momentum p_T for identified hadrons without string melting (left panel) and with melting melting (right panel). When assuming string melting the elliptic flow increases almost by a factor of 2 which results from a longer phase of partonic interactions during the early reaction phase.

PoS(CPOD2006)018

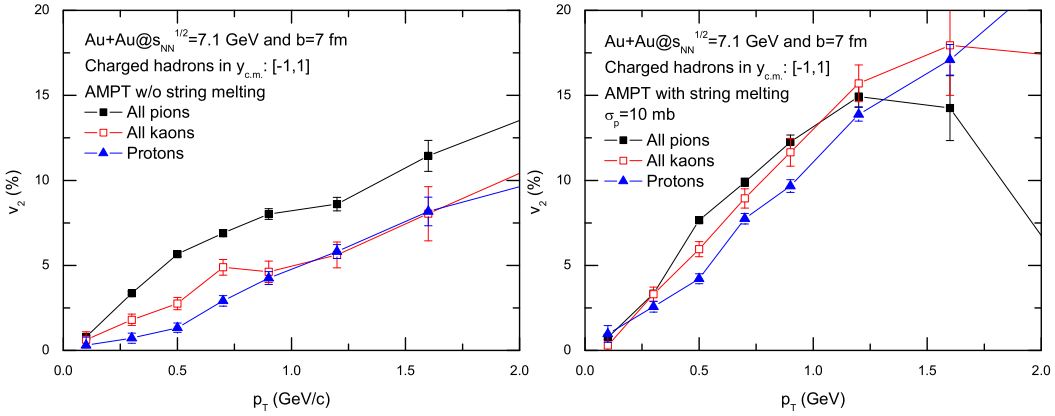

Figure 5: Strength of the elliptic flow strength for protons, pions and kaons as predicted by the AMPT code ([12]. Left panel: without string melting. Right panel: with string melting.

3.2 Low-mass vector mesons

The in-medium spectral functions of short-lived vector mesons - which are expected to be sensitive to chiral symmetry restoration - can be studied in the dense nuclear medium via their decay into lepton pairs [13]. Since the leptons interact only electromagnetically and hence are very little affected by the passage through the high-density matter, they provide, as a penetrating probe, almost undistorted information on the conditions in the interior of the collision zone.

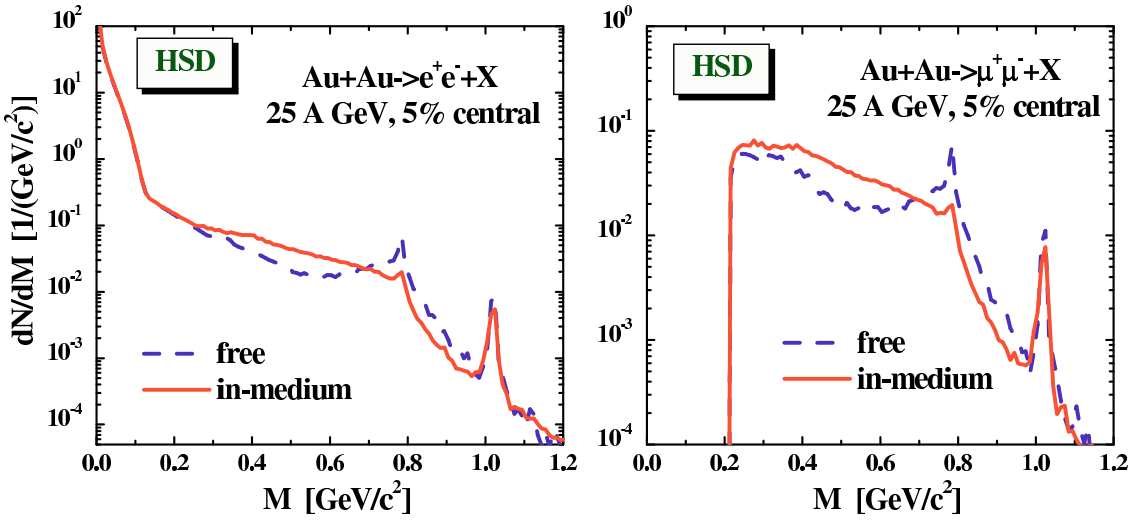

Figure 6: Yield of electron pairs (left panel) and muon pairs (right panel) as a function of invariant mass as predicted by the HSD transport code for central Au + Au collisions at 25 A·GeV [14]. Dashed lines: free vector meson spectral functions. Solid lines: in-medium spectral functions.

The question we have to answer is whether the measurement of electrons or muons is better suited for the identification of low-mass vector mesons in heavy-ion collisions at FAIR energies. In principle, both probes are sensitive to in-medium effects as illustrated in Figure 6 where HSD predictions are shown for the yields of electron-pairs (left panel) and muon pairs (right panel) as a function of invariant mass for central Au + Au collisions at 25 A·GeV [14]. The dashed lines

PoS(CPOD2006)018

represent the results for the free vector meson spectral functions, while the solid lines correspond to the in-medium scenario. The relative enhancement of the yield at low invariant masses due to the in-medium effects is very similar for electrons and muons. The experimental task is to reduce the combinatorial background which is due to Dalitz decays (pions and eta mesons) and gamma conversion in the case of electrons, and due to misidentified hadrons in the case of muons. For the measurement of high mass vector mesons such as J/ψ and ψ' the combinatorial background is much lower for muons than for electrons (see the last chapter).

3.3 Charm production

Charm production plays a particular role at FAIR energies, because charmonium, D-mesons and charmed hyperons are created at beam energies close to the kinematical threshold. Therefore, these particles are sensitive probes of the early, high-density stage of the collision (more than 10 times saturation density !). Collective effects contributing to charm production may be visible for the first time. Charm exchange processes may become important, revealing basic properties of charm propagation in a dense baryonic medium. The situation is analogue to strangeness production at SIS18 energies, where 2-3 times saturation density is probed in Au+Au collisions. In order to perform high statistics measurements, the low cross sections for charm production at threshold beam energies has to be compensated by high beam intensities. Figure 7 illustrates that no information on charm production is available in the FAIR energy range.

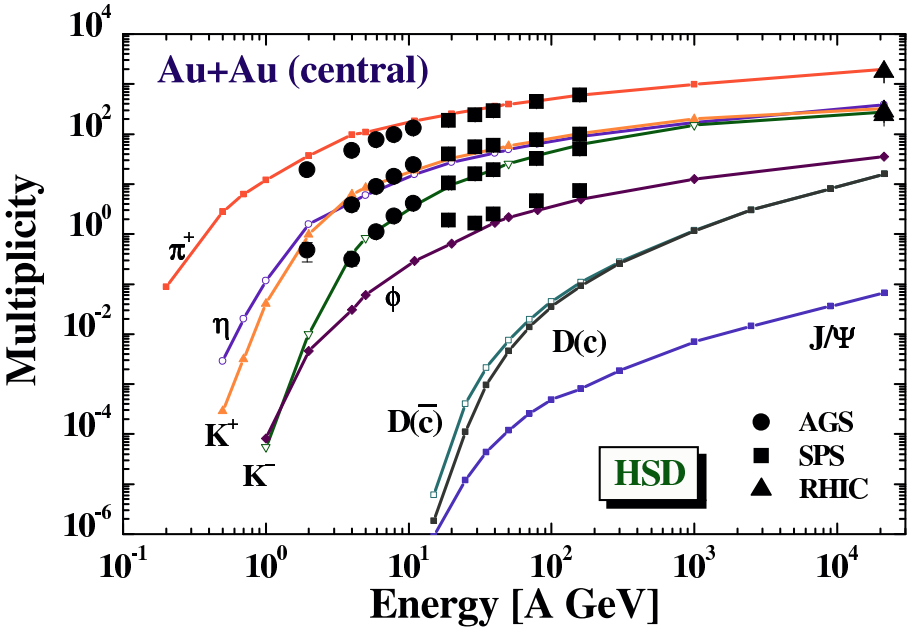

Figure 7: Multiplicities of π^+, η, K^+, K^-, ϕ, $D, \bar{D}$ and J/ψ-mesons for central collisions of Au+Au as a function of bombarding energy from SIS to RHIC energies. Solid lines: HSD predictions. Full symbols: measured data points (taken from ref. [15]).

The production of open charm is predicted to be sensitive to in-medium effects. The effective masses of D-mesons - a bound state of a heavy charm quark and a light quark - are expected to be modified in dense matter similarly to those of kaons. Such a change would be reflected in the

PoS(CPOD2006)018

relative abundance of charmonium ($c\bar{c}$) and D-mesons. This effect is illustrated in figure 8 where the transverse mass spectra of mesons is shown as calculated with the HSD transport code for central Au+Au collision at 25 A·GeV [14]. When taking into account an attractive DN potential (i.e. a mass shift of -50·ρ/ρ_0 MeV) the D-meson yield increases by almost one order of magnitude with respect to the calculation without in-medium effect.

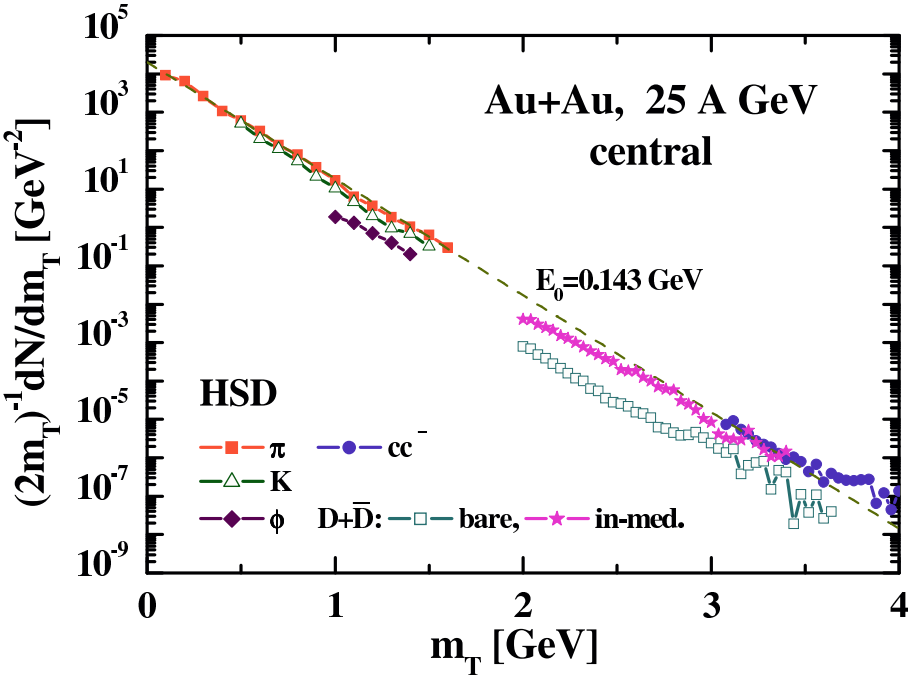

Figure 8: The transverss mass spectra of pions (full squares), kaons (open triangles), ϕ-mesons (full rhombes),$D+\bar{D}$ mesons (open squares) and $J/\psi, \psi'$ mesons (full dots) in the HSD approach for a central Au+Au collision at 25 A·GeV without including self energies for the mesons. The crosses stand for the D-meson m_T spectra when including an attractive mass shift of -50·ρ/ρ_0 MeV. The thin dashed line shows an exponential with slope parameter E_0 = 0.143 GeV. Note that final state elastic scattering of kaons and ϕ-mesons with pions has been discarded in the calculations.

4. The CBM detector

The experimental task is to identify both hadrons and leptons and to detect rare probes in a heavy ion environment. The apparatus has to measure multiplicities and phase-space distributions of hyperons, light vector mesons, charmonium and open charm (including the identification of protons, pions and kaons) with a large acceptance. The challenge is to filter out those rare probes in Au+Au (or U+U) collisions at reaction rates of up to 10 MHz. The charged particle multiplicity is about 1000 per central event. Therefore, the experiment has to fulfill the following requirements: fast and radiation hard detectors, large acceptance, lepton and hadron identification, high-resolution secondary vertex determination and a high speed trigger and data acquisition system. The layout of the CBM experimental setup is sketched in the right part of figure 9 together with the HADES detector (left part).

PoS(CPOD2006)018

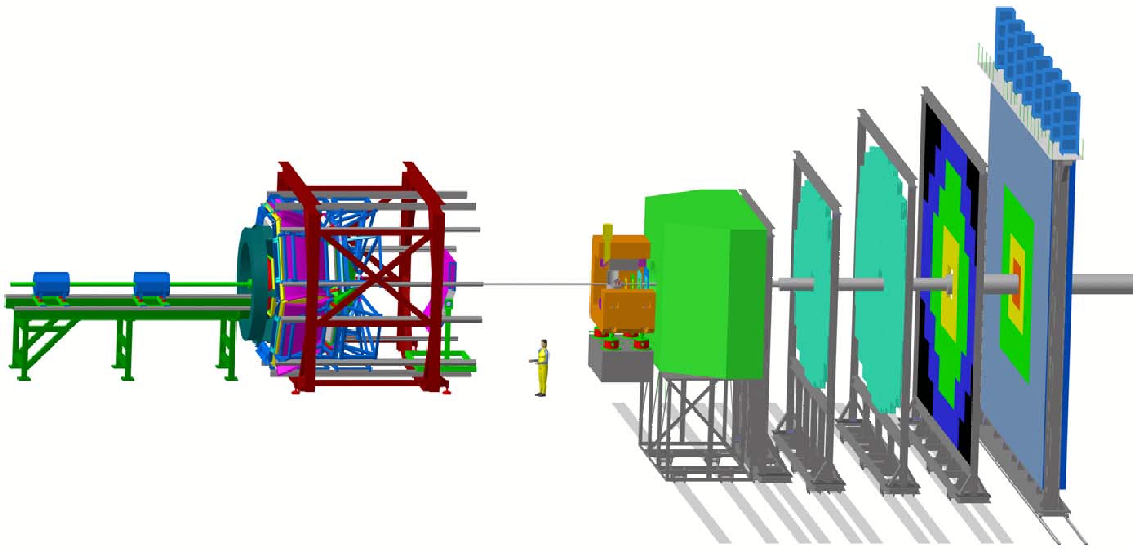

Figure 9: Sketch of the planned Compressed Baryonic Matter (CBM) experiment (right part) together with the HADES detector (left part). The CBM setup consists of a large acceptance superconducting dipole magnet, radiation-hard Silicon pixel/strip detectors for tracking and vertex determination, Ring imaging Cherenkov detectors (RICH) and Transition radiation detectors (TRD) for electron identification (or, alternatively, a muon detection system), Resistive plate counters (RPC) for time of flight measurement, an Electromagnetic calorimeter (ECAL) for identification of photons and neutral particles.

4.1 Hadron identification

The CBM detector accepts charged particles which are emitted at polar angles between 2 and 25 degrees in the laboratory. The resulting phase-space coverage for identified pions, kaons and protons produced in Au+Au collisions at 25 AGeV is illustrated in figure 10 as function of transverse momentum and rapidity.

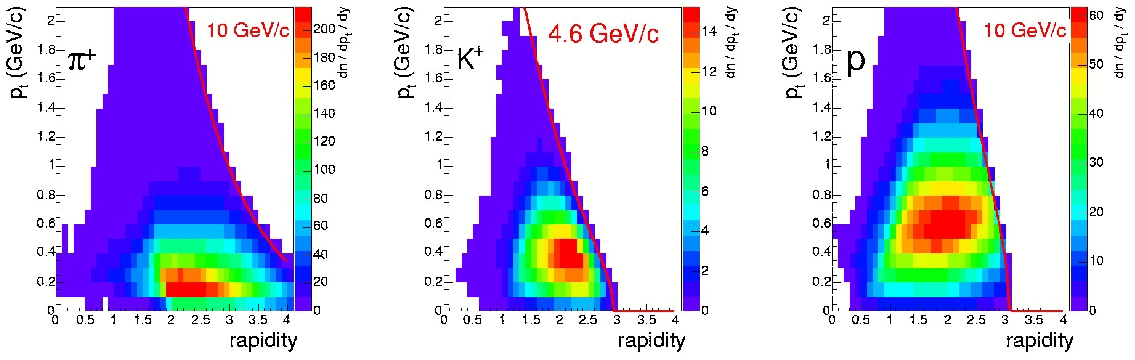

Figure 10: Acceptance of the CBM detector for identified pions, kaons and protons in the plane transverse-momentum versus rapidity as calculated for Au+Au at a beam energy of 25 AGeV. The particles are identified by time-of-flight assuming a time resolution of 80 ps for the RPC detector which is located 10 m downstream from the target.

PoS(CPOD2006)018

Hadron identification in the CBM experiment is performed in several steps. The first step is track reconstruction and momentum determination in the Silicon Tracking System. The efficiency for the reconstruction of primary tracks is presented in the left panel of figure 11. The second step is track reconstruction through the Transition Radiation Detector stations, and the third step is matching of the reconstructed tracks to hits in the RPC-TOF detector. The full reconstruction efficiency for hadrons (STS-TRD-RPC) is presented in the right panel of figure 11.

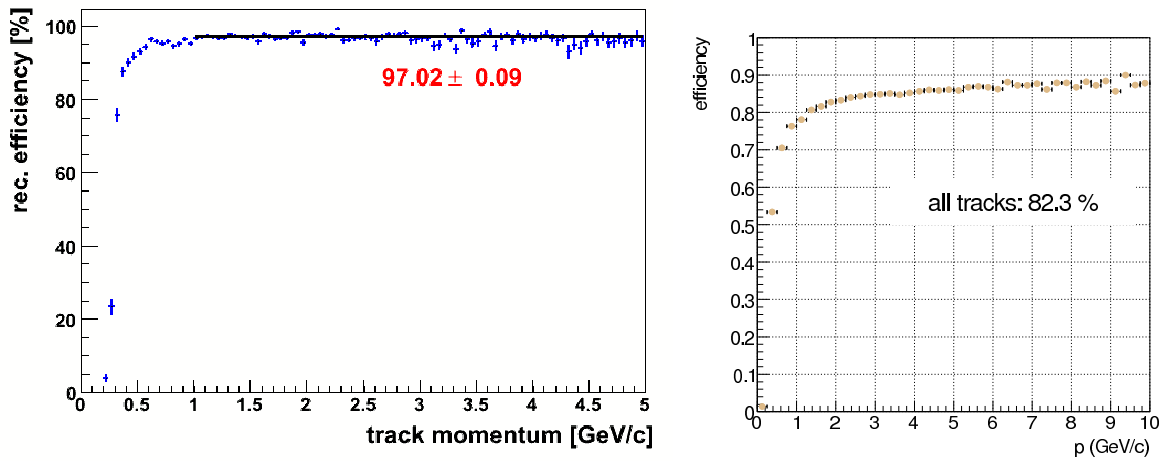

Figure 11: Track reconstruction efficiencies for the Silicon Tracking System (STS) (left panel) and for the combined STS-TRD-TOF system (right panel).

Hyperons can be identified via their decay topology using the STS information only. The results of simulations are shown figure 12.

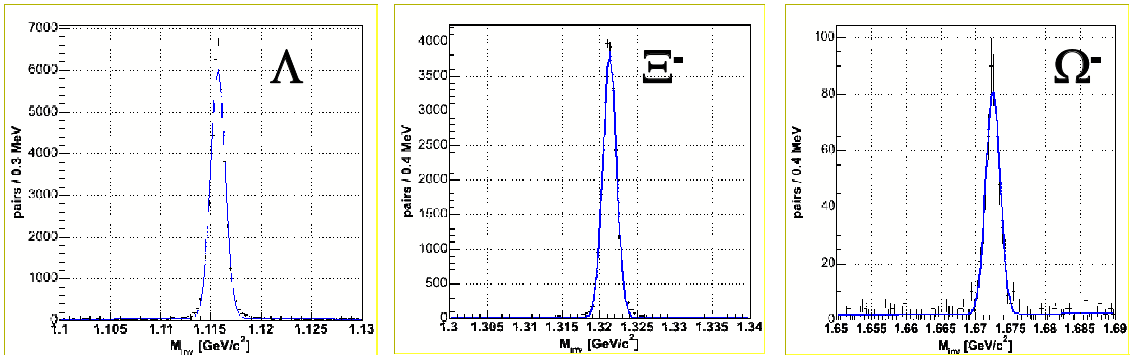

Figure 12: Invariant mass spectra of hyperons simulated for central Au+Au collisions at 25 AGeV using the UrQMD event generator. The particle are transported through the Silicon Tracking System using GEANT3, and the tracks are reconstructed using a Cellular Automaton algorithm for track finding and a Kalman filter for track fitting. No identification of the decay particles (protons and pions) has been performed. The background was suppressed by topological cuts. The reconstruction efficiency (including geometrical acceptance) is 15.8% for Lambdas, 6.7% for Xi, and 7.7% for Omegas.

PoS(CPOD2006)018

4.2 Open charm

In oder to identify D mesons via their hadronic decay ($D^0 \rightarrow K\pi$, $D^{\pm} \rightarrow K\pi\pi$) a high resolution Micro-Vertex Detector is required to suppress the background of kaons and pions emitted from the primary vertex. The performance of the Silicon Tracking System (STS) and the Micro-Vertex Detector (MVD) is illustrated in figure 13 which shows the invariant mass spectrum of a kaon and a pion simulated for Au+Au collisions at 25 AGeV. In this case the MVD consists of two Monolithic Active Pixel Sensors (MAPS) located at 10 cm and 20 cm downstream from the target, the STS consists of two Hybrid pixel detectors (at 30 cm and 40 cm) and 4 micro-strip layers (50 cm, 60 cm, 75 cm, 100 cm). The simulation has been performed within the CBMroot framework, using the UrQMD code to generate the background, and the GEANT3 code for transport. The result is based on track reconstruction using the Cellular Automaton algorithm for track finding and Kalman filter for track fitting, based on a realistic detector response.

The D^0 meson which has a lifetime of $\tau = 124\ \mu m/c$ is clearly visible without kaon and pion identification, but with proton rejection via time-of-flight measurement. Note that the first MAPS station is located 10 cm downstream from the target in order to reduce the radiation damage. The secondary vertex resolution improves significantly when the distance between target and the first MAPS is reduced. The signal-to-background ratio for D^+ meson is much better than for D^0 mesons, because their lifetime is longer ($\tau = 315\ \mu m/c$), and the combinatorial background is suppressed more efficiently as the secondary vertex is defined by 3 particles (one kaon and two pions).

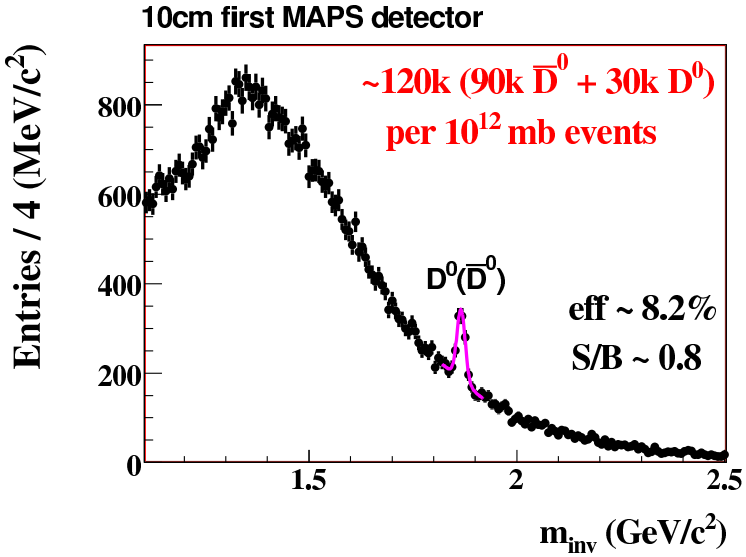

Figure 13: Invariant kaon-pion mass spectrum calculated for inclusive Au+Au collisions at 25 AGeV. The information from the micro-vertex detector (MVD) is used to reject particles emitted from the primary vertex. The first station of the MVD is located at 10 cm downstream from the target.

4.3 Identification of vector mesons via dileptonic decays

4.3.1 Electron measurements

Electrons and positrons are identified with the RICH detector and with the TRD. The radius of the produced Cherenkov rings are shown in the left panel of figure 14 as a function of the particle momentum for electrons and pions. The figure demonstrates that electrons can be distinguished from pions up to a momentum of about 9 GeV/c. In the right panel of figure 14 the energy loss of electrons and pions is shown for a single TRD layer for a particle momentum is 2 GeV/c.

PoS(CPOD2006)018

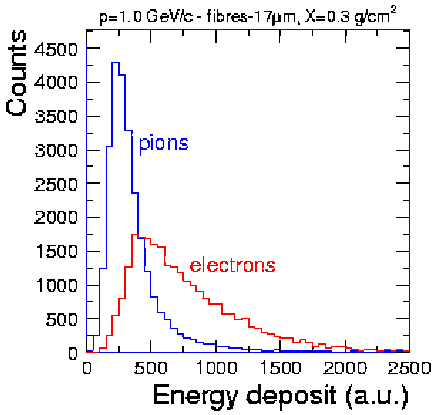

Figure 14: Left panel: RICH ring radius as function of momentum simulated with GEANT3 for electrons and pions. The radiator material is Nitrogen. Right panel: energy loss of pions and electrons in a single layer of the TRD.

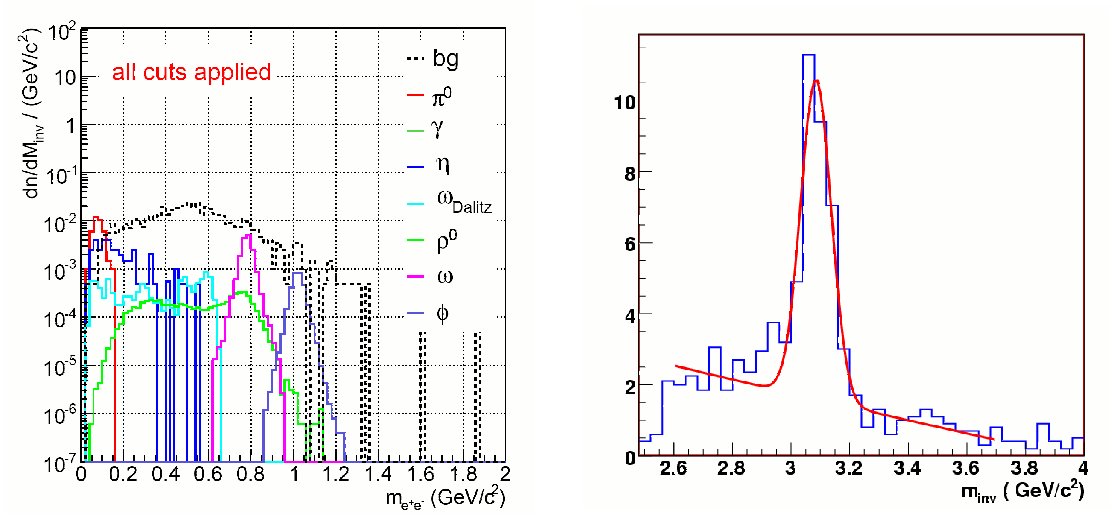

Figure 15: Invariant mass spectrum of electron-positron pairs for central Au+Au collisions at 25 AGeV using the UrQMD code for background generation and the HSD code for signal generation. Left panel: results of a MC simulation. Right panel: analysis based on track reconstruction (STS-TRD), on and electron identification using information from RICH (ring recognition and ring-track matching) and using energy loss signals in the TRD layers

The invariant mass distributions of electron-positron pairs are shown in figure 15 for central Au+Au collisions at 25 AGeV. The signals and the background are generated using the HSD and the UrQMD code, respectively. The left panel illustrates the results of a Monte Carlo simulation for low-mass vector mesons (based on ideal track reconstruction and ideal electron identification), where cuts have been applied in order to reduce the combinatorial background from pion Dalitz decays and gamma conversion. In the case of the J/ψ meson (right panel) full track reconstruction through STS and TRD has been performed. Moreover, the electrons have been identified using the information from the RICH (up to electron momenta of 9 GeV/c, based on ring-track matching and

PoS(CPOD2006)018

ring recognition algorithms), and performing an statistical analysis of the energy loss signals in 12 TRD layers. In the latter case the combinatorial background is reduced essentially by requiring a transverse momentum above 1 GeV/c for the single electrons and positrons.

4.3.2 Muon measurements

As an alternative approach to the dielectron measurement we have studied the possibility of detecting vector mesons (ρ, ω, ϕ, J/ψ) via their decay into $\mu^-\mu^+$ pairs. The idea is to suppress the hadrons with several absorber layers located just behind the Silicon Tracking System. In order to match the muons which pass the absorber to the tracks measured by the Silicon tracker (which define the momentum) one has to track all charged particles through the absorber. This is done by highly granulated and fast detectors which are located in each gap between the absorber layers.

The model of the muon detection system used in the GEANT3 transport code is displayed in figure 16. The 5 absorber layers consists of tungsten (5 cm), iron (10 cm + 20 cm +30 cm), and carbon (120 cm). The total thickness of the absorber corresponds to 7.3 nuclear interaction lengths. One muon detector is positioned in front of the first absorber, three detectors are located in each of the 4 gaps in between the absorber layers, and 3 detectors are located behind the last absorber. The experimental challenge for the detectors and the track reconstruction routines is the particle hit density of about 1 /cm^2 per event in the first detector layers.

Figure 16 does not show the RPC-TOF wall located 10 m downstream from the target, the intermediate tracking chambers between muon detection system, and the electromagnetic calorimeter. For hadron measurements the absorber layers will be removed and the muon chambers can be used as hadron tracking detectors.

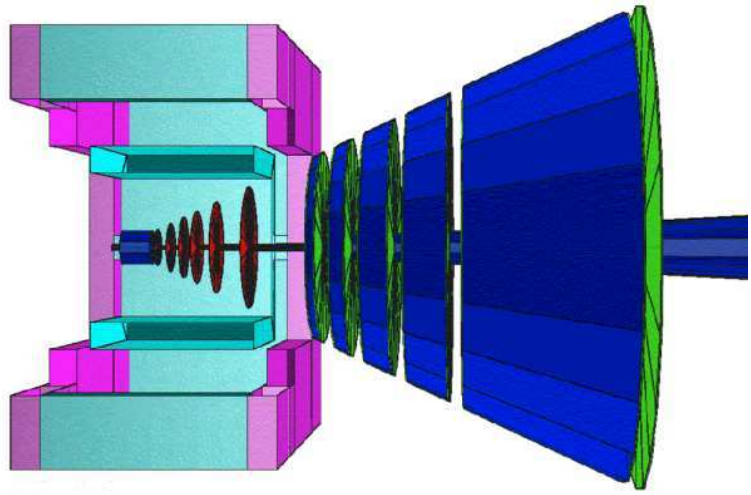

Figure 16: Sketch of the CBM Muon detection system consisting of the STS in the magnetic dipole field, followed by 5 layers of absorbers and 16 layers of tracking detectors.

Feasibility studies have been performed within the CBMroot simulation software package, using the UrQMD code as event generator and the GEANT3 code for transporting the events through the model of the muon detection system. The simulations are based on track reconstruction algorithms taking into account a realistic response of the Silicon pixel and strip detectors (STS). The position resolution of the muon tracking detectors is assumed to be $\sigma = 100\mu m$. Reconstructed

PoS(CPOD2006)018

charged particle tracks with hits in the last three muon chambers located behind the absorber are associated with muons. The performance of the CBM muon detector system is illustrated in figure 17 which shows the invariant dimuon mass spectrum calculated for inclusive Au+Au collisions at 25 AGeV. A signal-to-background ratio of about 100 can be achieved in the region of the J/ψ peak, a value which should be sufficient to identify even the ψ' meson.

Further simulations are needed to decide whether electron or muon detection is better suited for the measurement of the leptonic decay of vector mesons. Electron pairs have the advantage that the very low invariant mass region is accessible if the large combinatorial background can be suppressed. For muon pairs the available phase space is strongly reduced at invariant masses below 500 MeV/c^2. On the other hand, for invariant masses above about 1 MeV/c^2 the signal-to background ratio is much larger for muon pairs than for electron pairs.

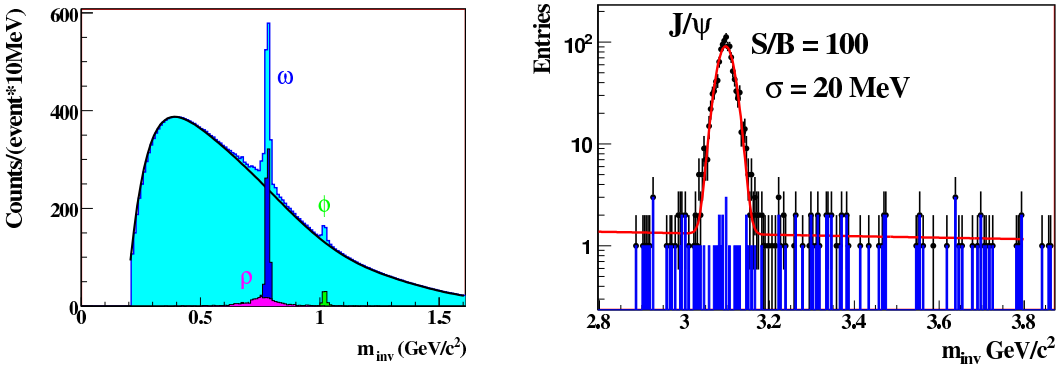

Figure 17: Invariant dimuon mass spectra calculated for Au+Au minimum bias collisions at 25 AGeV. The simulation has been performed within the CBMroot framework, using the UrQMD code to generate the background, and the GEANT3 code for transport. The result is based on track reconstruction. The ψ' meson was not included in the simulation.

The CBM detector is designed for a comprehensive research program using proton beams (with energies of 10 - 90 GeV) and nuclear beams (10 - 45 AGeV) impinging on various targets. The measurements at beam energies below 10 AGeV will be performed with the HADES detector. The measurements, in particular those of rare diagnostic probes, require a dedicated accelerator with high beam intensities, large duty cycle, excellent beam quality, and with an operational availability of several month per year. Details of the CBM research program and of the setup can be found in the Technical Status Report which has been submitted in January 2005 [16]. The CBM Collaboration actually consists of about 350 persons from 41 institutions and 15 countries.

5. Acknowledgements

We acknowledge the contributions of our colleagues Supriya Das, Volker Friese, Sergei Gorbunov, Johann Heuser, Claudia Höhne, Ivan Kisel, Alla Maevskaya, Walter F.J. Müller, Iouri Vassiliev. We thank Elena Bratkovskaya, Christian Fuchs and Jorgen Randrup for their contributions to theory. CBM project is supported by EU under RII3-CT-2004-506078 HADRONPHYSICS and by INTAS Ref. Nr. 03-51-6645.

PoS(CPOD2006)018

References

[1] FAIR Conceptional Design Report 2001,

`http://www.gsi.de/GSI-Future/cdr/`

[2] F. Weber, J. Phys. G:, Nucl. Part. Phys. **27** (2001) 465

[3] F. Wilczek, Physics Today **53** (2000) 22

[4] M. Stephanov, K. Rajagopal, E. Shuryak, Phy. Rev. **D 60** (1999) 114028

[5] K. K. Gudima, M. Ploszajczak and V. D. Toneev, Phys. Lett. B 328 (1994) 249; L. Bravina et al., Phys. Lett. B 631 (2005) 109; G. Burau et al., Phys.Rev. C71 (2005) 054905 J. Bleibel et al., Nucl. Phys. A 767 (2006) 218;

[6] Y. Ivanov, V. Russkikh, V.Toneev, Phys.Rev. C73 (2006) 044904

[7] Z. Fodor and S.D. Katz, JHEP **0404** (2004) 050

[8] S. Ejiri et al., hep-lat/0312006, Prog.Theor.Phys.Suppl. 153 (2004) 118

[9] C. Blume et al., J. Phys. **G 31** (2005) 685

[10] J. Randrup and J. Cleymans, hep-ph/0607065

[11] C. Blume, J. Phys. G 31 (2005) S57.

[12] B. Zhang et al, Phys. Rev. C 61 (2000) 067901; Z.W. Lin et al, Phys. Rev. C 64 (2001) 011902; Z. W. Lin *et al.*, Nucl. Phys. A 698 (2002) 375.

[13] R. Rapp and J. Wambach, Nucl. Phys. **A 661** (1999) 33c

[14] E.L. Bratkovskaya, private communication

[15] W. Cassing, E. L. Bratkovskaya, and A. Sibirtsev, Nucl. Phys. A 691 (2001) 753.

[16] CBM Technical Status Report 2005

`http://www-linux.gsi.de/~hoehne/report/cbmtsr_public.pdf`

PoS(CPOD2006)018